



# OPEN An AC voltage sensorless predictive current control method for grid-tied inverter with enhanced robustness against current DC offset

Guolin Zhang<sup>1</sup>, Weidong Dong<sup>2</sup>✉, Lingfeng Meng<sup>2</sup>, Jinyuan Li<sup>2</sup> & Jiqiang Wang<sup>2</sup>

Conventional AC voltage sensorless predictive current control methods for grid-tied inverter are often sensitive to current DC offset errors, resulting in worse control performance. To solve this problem, this paper proposed an improved grid voltage observer as well as a new lumped DC offset observation method. First, the drawbacks of the conventional grid voltage observer are reviewed. Then, based on the backstepping design approach, an improved grid voltage observer is designed, which can remove the influences of the current DC offsets. Third, the effects of the current DC offset on the current control is analyzed, and a new lumped DC offset observation method is designed, which can estimate and compensate the current DC offset well. Fourth, based on the two proposed observers, a new AC voltage sensorless predictive current control method is achieved with enhanced robustness against current DC offset. Finally, experimental studies are carried out, which verify the strong robustness against current DC offsets of the proposed method.

**Keywords** AC voltage sensorless, DC offset, Grid voltage observer, Lumped DC offset observer, Backstepping design approach

To relieve environmental pollution problems, realize the sustainable development, renewable energy technologies have received more and more attentions over the whole world<sup>1–4</sup>. To transfer the power generated by wind, photovoltaic, or other energy sources to electrical supply smoothly, new power electronic technologies and new control theories have been widely studied and applied to control the grid-tied inverters<sup>5,6</sup>, aiming to transfer the DC voltage to AC voltage steadily.

The classical control methods for grid-tied inverters are grid voltage-oriented vector control methods and direct power control methods<sup>7</sup>. The former method usually has a complicated control structure with several key parameters that should be tuned carefully. The latter method often has large current and power ripples at steady state. As a result, new methods with improved control performance require to be further developed.

In recent days, many researchers over the world have studied lots of different kinds of new control technologies for grid-tied inverters, including sliding mode control technologies<sup>8</sup>, active disturbance rejection control technologies<sup>9</sup>, model predictive control technologies<sup>10–14</sup>, and so on. Among them, model predictive control technology has been widely studied by many researchers from China and abroad since this kind of method has a lot of advantages<sup>15,16</sup>, overcoming the main drawbacks of the classical control methods<sup>7</sup>.

In<sup>17,18</sup>, the principles and developments of model predictive control technology are reviewed. It is shown that many sensors are required for this control system, such as the encoders, the AC current sensors, the DC voltage sensors, and AC voltage sensors, etc. For grid-tied inverters, AC voltage sensors are often required to measure the three-phase grid voltages, which are the basis of grid voltage-oriented control and model predictive control<sup>19</sup>. It is known that the fault of the AC voltage sensors often results in the shutting down of the grid-tied inverters, reducing the stability of the renewable energy generation systems heavily. Thus, it is very meaningful to study AC voltage sensorless predictive current control methods for grid-tied inverter using new methods<sup>20–26</sup>.

<sup>1</sup>GD Power Development Co.,LTD, Beijing 100101, China. <sup>2</sup>Guodian Electric Power Qingneng Etoke Front Banner Co., LTD, Erdos 017000, China. ✉email: Power\_11111@163.com

In<sup>20</sup>, a second order sliding mode observer is designed to observe the grid voltages, and a new frequency adaptive grid voltage compensation method is proposed, overcoming the influences of the frequency deviation. However, this method is sensitive to current DC offset error. Once there is some DC errors generated by the current sampling circuits, there will be some obvious grid voltage observation errors, resulting in poor current control performance. In<sup>21</sup>, the virtual flux, instead of the grid voltage, is observed by designing a virtual flux sliding mode observer. However, it is still sensitive to the unwanted DC errors. In<sup>22</sup>, to achieve AC voltage sensorless control, the virtual flux is observed by designing an observer in time-domain. To overcome the influences of the unwanted DC errors, an error-compensation mechanism is presented. In<sup>23</sup>, to achieve AC voltage sensorless control, another virtual flux observer is constructed by introducing a band-stop filter feedback to solve the influences of the DC bias. However, for model predictive control of grid-tied inverters, the grid voltages are required for the current prediction model, which cannot be directly provided by the virtual flux observers. In<sup>24</sup>, grid voltage sensorless control is achieved for pulse width modulation rectifiers by designing a novel grid voltage phase angle estimation method. However, this kind of method only works at unity power factor operation condition. In<sup>25</sup>, a sliding mode grid voltage observer is developed, which can track the actual grid voltage accurately without phase lag and magnitude error. Although it can reduce the influences of the unwanted DC errors to a certain extent, the influences cannot be eliminated. Moreover, in this paper, the influences of the DC errors on the predictive current control are not considered.

It is known that the predictive current control performance of grid-tied inverters relies on the accurate current feedbacks<sup>26,27</sup>. Once there are some DC errors, the current control performance will be reduced. To solve this problem, many papers studied the estimation and compensation methods of current DC errors<sup>28–32</sup>. In<sup>28</sup>, the effects of the current DC errors on the current control loop are analyzed, and a DC error compensation method is proposed based on the current control error on the synchronous reference frame. In<sup>29</sup>, further improvement is made by considering the effects of the saturation of current controller. In<sup>30</sup>, a PI-type observer is designed for the estimation of the current offset error, and a DC error compensation method is also designed to remove the effects on the current control. In<sup>31</sup>, an adaptive extended state observer is further developed to compensate the current measurement DC offset error without additional hardware. In<sup>32</sup>, a D-axis flux estimator is modified to achieve the estimation and compensation of the current DC errors. Although all the methods designed in<sup>28–32</sup> work well, they cannot be applied for AC voltage sensorless predictive current control of grid-tied inverters since there are no grid voltage sensors.

Up to now, few papers have studied the AC voltage sensorless predictive current control methods for grid-tied inverters by considering both the influences of the current DC offset on the grid voltage observation and on the current predictive control performance. To fill this gap, an AC voltage sensorless predictive current control method for grid-tied inverter with enhanced robustness against current measurement DC offset error is proposed in this paper.

The main contributions of this paper lie in two aspects.

In one aspect, a new grid voltage observer is proposed, which can observe the grid voltage without static error even under large current DC offset conditions.

In another aspect, a new current DC offset estimation and compensation method is designed, which can eliminate the effects of the current DC offset on the predictive current control system.

Finally, simulation and experimental studies are carried out, which verify the effectiveness of the proposed methods in this paper.

## Description of the system

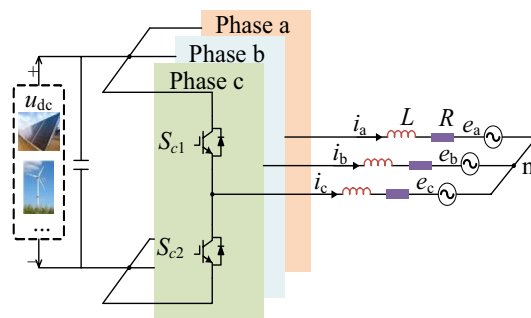
### Mathematical model of the grid-tied inverter

Figure 1 depicts the topology of the grid-tied inverter.

According to Fig. 1, the mathematical model of the grid-tied inverter can be expressed as

$$L \frac{di_{abc}}{dt} = u_{abc} - Ri_{abc} - e_{abc} \quad (1)$$

where  $L$  is the filter inductance,  $R$  is the resistance on the  $L$ ,  $i_{abc} = [i_a, i_b, i_c]^T$  is the grid current,  $e_{abc} = [e_a, e_b, e_c]^T$  is the grid voltage, and  $u_{abc} = [u_a, u_b, u_c]^T$  is the output voltage of the inverter.



**Fig. 1.** Topology of the grid-tied inverter.

To simplify this model, (1) can be transformed to the stationary  $\alpha\beta$  reference frame<sup>33</sup>, and it is deduced that

$$L \frac{di_{\alpha\beta}}{dt} = u_{\alpha\beta} - Ri_{\alpha\beta} - e_{\alpha\beta} \tag{2}$$

where  $i_{\alpha\beta} = [i_{\alpha}, i_{\beta}]^T$ ,  $e_{\alpha\beta} = [e_{\alpha}, e_{\beta}]^T$  and  $u_{\alpha\beta} = [u_{\alpha}, u_{\beta}]^T$  are the grid current, grid voltage, and output voltage of the inverter on the stationary  $\alpha\beta$  reference frame.

### Principle of the predictive current control system

The principle of the model predictive control system has been explained in many papers<sup>34</sup>, which includes the prediction of the current at  $k+1$  instant using the last optimal voltage vector, the prediction of the current at  $k+2$  instant using the eight voltage vectors generated by the grid-tied inverter at current instant, the calculation of the cost function corresponding to the eight voltage vectors, and the selection of the optimal voltage vector by comparing the values of the cost function. Figure 2 is given here to show the principle of the model predictive control system more clearly, where  $M = 1 - R/L^*T_s$ ,  $N = 1/L^*T_s$ ,  $U_{\alpha}(k) = u_{\alpha}(k) - e_{\alpha}(k)$ ,  $U_{\beta}(k) = u_{\beta}(k) - e_{\beta}(k)$ ,  $U_{\alpha}(k+1) = u_{\alpha}(k+1) - e_{\alpha}(k+1)$ , and  $U_{\beta}(k+1) = u_{\beta}(k+1) - e_{\beta}(k+1)$ .

Besides, it should be noted that reference current  $i_{\alpha}^*$  and  $i_{\beta}^*$  in the cost function can be calculated according to reference current  $i_d^*$  and  $i_q^*$  on the synchronous rotating dq reference frame stationary, which meet

$$\begin{cases} i_{\alpha}^* = i_d^* \cos \theta - i_q^* \sin \theta \\ i_{\beta}^* = i_d^* \sin \theta + i_q^* \cos \theta \end{cases} \tag{3}$$

where  $\theta$  is the phase angle of the grid voltage.

According to the step 2 and 3 in Fig. 2, it is found that the prediction of the current at  $k+1$  instant and  $k+2$  instant relies on the sampled grid voltages using AC voltage sensors. Meanwhile, according to step 4 and (3), it is seen that the phase angle of grid voltage is also needed for the calculation of the reference current, which also should be estimated according to the sampled grid voltages using AC voltage sensors. As a result, it is concluded that the model predictive control of grid-tied inverter relies on the accurate sampled grid voltages heavily. To ensure the operational stability of the grid-tied inverter under the fault of AC voltage sensors, AC voltage sensorless control methods, which use the estimated grid voltages to replace the sampled ones, require to be designed urgently.

### Review of the conventional grid voltage observation method

In<sup>25</sup>, a sliding mode grid voltage observer is designed to achieve AC voltage sensorless predictive current control. Here, this observer is reviewed and analyzed.

### Conventional grid voltage observer

Under ideal conditions, the grid voltage can be assumed as a sinusoidal signal without harmonic. So, it can be deduced that

$$\frac{de_{\alpha\beta}}{dt} = j\omega e_{\alpha\beta} \tag{4}$$

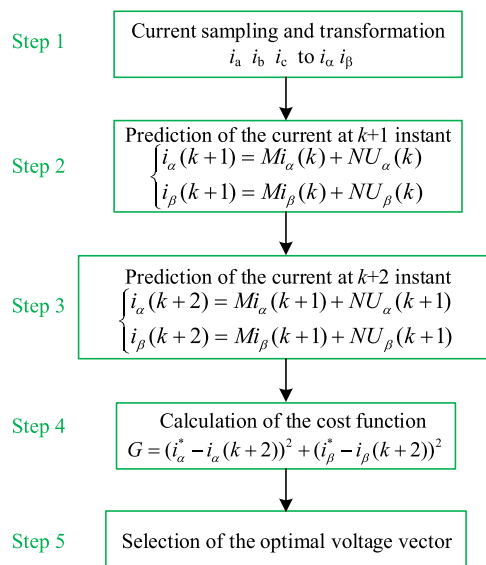


Fig. 2. Principle of the model predictive control system.

where  $\omega$  denotes the frequency of the grid voltage.

Based on (2) and (4), a sliding mode grid voltage observer can be designed as

$$\begin{cases} \frac{d\hat{i}_{\alpha\beta}}{dt} = \frac{1}{L}(\mathbf{u}_{\alpha\beta} - R\hat{i}_{\alpha\beta} - \hat{e}_{\alpha\beta} + k_1 \text{sgn}(i_{\alpha\beta} - \hat{i}_{\alpha\beta})) \\ \frac{d\hat{e}_{\alpha\beta}}{dt} = j\omega\hat{e}_{\alpha\beta} - k_2 \text{sgn}(i_{\alpha\beta} - \hat{i}_{\alpha\beta}) \end{cases} \quad (5)$$

where  $\hat{i}_{\alpha\beta} = [\hat{i}_\alpha, \hat{i}_\beta]^T$  is the estimated grid current,  $\hat{e}_{\alpha\beta} = [\hat{e}_\alpha, \hat{e}_\beta]^T$  is the observed grid voltage,  $k_1$  and  $k_2$  are the observer gains.

Since a detailed stability analysis has been carried out in<sup>25</sup>, and it is not repeated here.

**Feature analysis**

According to<sup>25</sup>, the transfer function of the conventional sliding mode grid voltage observer can be deduced as

$$G_1 = \frac{\hat{e}_{\alpha\beta}}{e_{\alpha\beta}} = \frac{\lambda}{s - j\omega + \lambda} \quad (6)$$

where  $\lambda = k_2/k_1$ .

According to (6) it is easy to found that

$$G_{1(s=j\omega)} = \frac{\lambda}{j\omega - j\omega + \lambda} = 1 \angle 0^\circ \quad (7)$$

Equation (7) means that the conventional sliding mode grid voltage observer can observe the grid voltage accurately without steady state error.

Meanwhile, according to (6) it is easy to found that

$$G_{1(s=0)} = \frac{\lambda}{0 - j\omega + \lambda} = \frac{1}{\sqrt{(\omega/\lambda)^2 + 1}} \angle \tan^{-1} \frac{\omega}{\lambda} \quad (8)$$

Equation (8) means that for the DC offset signal, the amplitude and phase generated by the conventional sliding mode grid voltage observer are both not equal to zero, indicating that if there are some unwanted DC offset signals, the observed grid voltage will be affected. Moreover, from (8) it can be further concluded that a smaller  $\lambda$  can be used to reduce the influences of the unwanted DC offset signals.

Additionally, according to (6) it is easy to found that

$$G_{1(s=j\omega_h)} = \frac{\lambda}{j\omega_h - j\omega + \lambda} = \frac{1}{\sqrt{((\omega_h - \omega)/\lambda)^2 + 1}} \angle \tan^{-1} \frac{\omega - \omega_h}{\lambda} \quad (9)$$

where  $\omega_h$  is the frequency of the high frequency signal.

Equation (9) means for the high frequency signal, the amplitude and phase generated by the conventional sliding mode grid voltage observer are also both not equal to zero, indicating that if there are some unwanted high frequency signals, the observed grid voltage will also be affected. Furthermore, similar to (8), from (9) it is deduced that a smaller  $\lambda$  is preferred since the influences of the unwanted high frequency signals can be reduced.

However, although from (8)-(9) it is found that a smaller  $\lambda$  is preferred, the dynamic control performance of the conventional sliding mode grid voltage observer will be reduced if  $\lambda$  is small. To show the effects of  $\lambda$ , the bode diagram of  $G_1$  is plotted with different values of  $\lambda$ , which is shown in Fig. 3.

It is seen from Fig. 3 that the conventional grid voltage observer has a weak band-pass feature. When  $\lambda$  is small, the bandwidth is also small, meaning the dynamic control performance is weak, while the DC offset

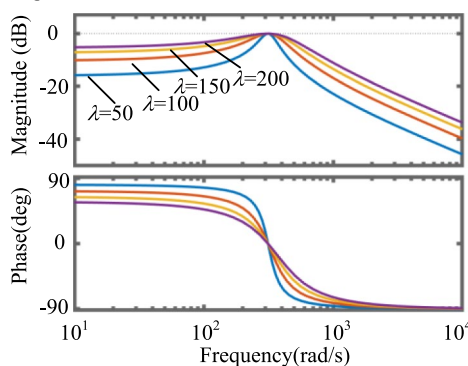


**Fig. 3.** Bode diagram of  $G_1$ .

and high frequency signal suppression ability are strong. When  $\lambda$  is enlarged, the bandwidth is increased too. However, the DC offset and high frequency signal suppression ability are reduced.

From the above analysis, it is seen that  $\lambda$  is difficult to be selected to get both better bandwidth and better DC offset and high frequency signal suppression ability. That's the drawback of the conventional grid voltage observer. Moreover, although a smaller  $\lambda$  can be selected to enhance the DC offset suppression ability, the influences of the DC offset on the grid voltage observation cannot be eliminated. That's another the drawback of the conventional grid voltage observer.

### Proposed grid voltage observation method

As analyzed in Sect. "Description of the system", the accurate information of the grid voltage is the key to achieve satisfactory AC voltage sensorless predictive current control for grid-tied inverter. Although some papers have studied grid voltage observation methods, they are sensitive to DC offset. In this Section, an improved is designed based on the backstepping design approach, aiming at estimating the grid voltage without static error with enhanced insensitiveness to DC offset.

### Design of improved grid voltage observer

First, the conventional sliding mode grid voltage observer shown in (5) is revised as (10), where  $\eta$  is a parameter that provides a new degree of freedom to design the observer immune to DC offset.

$$\begin{cases} \frac{d\hat{i}_{\alpha\beta}}{dt} = \frac{1}{L}(u_{\alpha\beta} - R\hat{i}_{\alpha\beta} - \hat{e}_{\alpha\beta} + k_1 \text{sgn}(i_{\alpha\beta} - \hat{i}_{\alpha\beta})) \\ \frac{d\hat{e}_{\alpha\beta}}{dt} = \eta\hat{e}_{\alpha\beta} - k_2 \text{sgn}(i_{\alpha\beta} - \hat{i}_{\alpha\beta}) \end{cases} \quad (10)$$

According to (2), and (10), it can be deduced that

$$\frac{d(i_{\alpha\beta} - \hat{i}_{\alpha\beta})}{dt} = \frac{1}{L}(-R(i_{\alpha\beta} - \hat{i}_{\alpha\beta}) - e_{\alpha\beta} + \hat{e}_{\alpha\beta} - k_1 \text{sgn}(i_{\alpha\beta} - \hat{i}_{\alpha\beta})) \quad (11)$$

When the current zero reduces to zero at steady state, it can be calculated that

$$\hat{e}_{\alpha\beta} - e_{\alpha\beta} = k_1 \text{sgn}(i_{\alpha\beta} - \hat{i}_{\alpha\beta}) \quad (12)$$

Then, substituting (12) into the second equation of (10), it is obtained that

$$\frac{d\hat{e}_{\alpha\beta}}{dt} = \eta\hat{e}_{\alpha\beta} - \frac{k_2}{k_1}(\hat{e}_{\alpha\beta} - e_{\alpha\beta}) \quad (13)$$

Based on (13), it is further deduced that

$$G_2 = \frac{\hat{e}_{\alpha\beta}}{e_{\alpha\beta}} = \frac{\lambda}{s - \eta + \lambda} \quad (14)$$

Based on (14) and (6), it is easy to find that if  $\eta = j\omega$ , the observer shown in (10) will be the same as the conventional one. However, as analyzed before, this observer cannot eliminate the effects of DC offset. So, here,  $\eta$  is redesigned based on the backstepping design approach, aiming at estimating the grid voltage without static error with enhance insensitiveness to DC offset.

Here, a transfer function  $G_3$  shown in (15) is predesigned since it can eliminate the impacts of DC offset<sup>35</sup>.

$$G_3 = \frac{\lambda s}{s^2 + \lambda s + \omega^2} \quad (15)$$

Then, based on the backstepping design approach, it is assumed that  $G_2 = G_3$ . Thus, it is easy to deduced that

$$\eta = -\frac{\omega^2}{s} \quad (16)$$

Finally, by substituting (16) into (10), an improved sliding mode grid voltage observer is designed, as shown below.

$$\begin{cases} \frac{d\hat{i}_{\alpha\beta}}{dt} = \frac{1}{L}(u_{\alpha\beta} - R\hat{i}_{\alpha\beta} - \hat{e}_{\alpha\beta} + k_1 \text{sgn}(i_{\alpha\beta} - \hat{i}_{\alpha\beta})) \\ \frac{d\hat{e}_{\alpha\beta}}{dt} = -\frac{\omega^2}{s}\hat{e}_{\alpha\beta} - k_2 \text{sgn}(i_{\alpha\beta} - \hat{i}_{\alpha\beta}) \end{cases} \quad (17)$$

### Stability analysis

To ensure the stability of the proposed grid voltage observer, theoretical analysis is carried out here based on the Lyapunov theory.

First, a Lyapunov function is designed as (18) to ensure the stability of the current observer.

$$V_1 = \frac{1}{2}(\mathbf{i}_{\alpha\beta} - \hat{\mathbf{i}}_{\alpha\beta})^2 \tag{18}$$

Then, it is deduced that

$$\frac{dV_1}{dt} = -\frac{R}{L}(\mathbf{i}_{\alpha\beta} - \hat{\mathbf{i}}_{\alpha\beta})^2 + A \tag{19}$$

where  $A = \frac{1}{L}(\mathbf{i}_{\alpha\beta} - \hat{\mathbf{i}}_{\alpha\beta})(\hat{\mathbf{e}}_{\alpha\beta} - \mathbf{e}_{\alpha\beta} - k_1 \text{sgn}(\mathbf{i}_{\alpha\beta} - \hat{\mathbf{i}}_{\alpha\beta}))$ .

To ensure the stability of the observer,  $dV_1/dt$  should be less than zero. So, the term  $A$  can be designed to be less than zero.

When  $\mathbf{i}_{\alpha\beta} - \hat{\mathbf{i}}_{\alpha\beta} > 0$ , it can be deduced that

$$A = \frac{1}{L}(\mathbf{i}_{\alpha\beta} - \hat{\mathbf{i}}_{\alpha\beta})(\hat{\mathbf{e}}_{\alpha\beta} - \mathbf{e}_{\alpha\beta} - k_1) < 0 \tag{20}$$

So, it is calculated that

$$k_1 > \hat{\mathbf{e}}_{\alpha\beta} - \mathbf{e}_{\alpha\beta} \tag{21}$$

Similarly, when  $\mathbf{i}_{\alpha\beta} - \hat{\mathbf{i}}_{\alpha\beta} < 0$ , it can be deduced

$$k_1 > -(\hat{\mathbf{e}}_{\alpha\beta} - \mathbf{e}_{\alpha\beta}) \tag{22}$$

As a result, it is concluded that

$$k_1 > |\hat{\mathbf{e}}_{\alpha\beta} - \mathbf{e}_{\alpha\beta}| \tag{23}$$

Then, the stability of the grid voltage observer shown in the second equation of (10) is analyzed, whose transfer function is (15). According to (15), it is easy to deduce that  $\lambda$  should be larger than 0 to make the poles on the left side of the  $s$ -plane. Thus, since  $k_1$  is larger than zero according to (25),  $k_2 > 0$  is deduced. So, the proof is completed.

### Feature analysis

From the above deduction, it is known that the transfer function of the proposed grid voltage observer is depicted as (15).

According to (15) it is easy to found that

$$G_{3(s=j\omega)} = \frac{\lambda j\omega}{-\omega^2 + \lambda j\omega + \omega^2} = 1\angle 0^\circ \tag{24}$$

Equation (24) means that the proposed grid voltage observer also can observe the grid voltage accurately without steady state error, which is the same with the conventional method.

Meanwhile, according to (15) it is easy to found that

$$G_{3(s=0)} = \frac{\lambda 0}{0^2 + \lambda 0 + \omega^2} = 0\angle 0^\circ \tag{25}$$

Equation (25) that means for the DC offset signal, the amplitude and phase generated by the proposed grid voltage observer are both equal to zero, indicating that the proposed grid voltage observer is immune to DC offset, which overcomes the drawbacks of the conventional method.

Additionally, it is also easy to found that

$$G_{1(s=j\omega_h)} = \frac{\lambda s}{s^2 + \lambda s + \omega^2} = \frac{1}{\sqrt{((\omega^2 - \omega_h^2)/(\lambda\omega_h))^2 + 1}} \angle \frac{\pi}{2} - \tan^{-1} \frac{\lambda\omega_h}{\omega^2 - \omega_h^2} \tag{26}$$

Equation (26) means that for the high frequency signal, the amplitude and phase generated by the proposed grid voltage observer are not equal to zero, indicating that if there are some unwanted high frequency signals, the observed grid voltage will also be affected. Furthermore, similar to (9), from (26) it is deduced that a smaller  $\lambda$  is preferred since the influences of the unwanted high frequency signals can be reduced.

To further evaluate and compare the performance of the proposed grid voltage observer with the conventional method, the bode diagram of  $G_3$  is plotted with different values of  $\lambda$ , which is shown in Fig. 4.

Different from Fig. 3, it is seen from Fig. 4 that the proposed grid voltage observer has a strong band-pass feature. No matter how large  $\lambda$  is, the proposed grid voltage observer always has a low gain for the DC offset. That's because  $G_{3(s=0)}$  is always equal to zero, as analyzed in (25), indicating that the influences of the DC offset

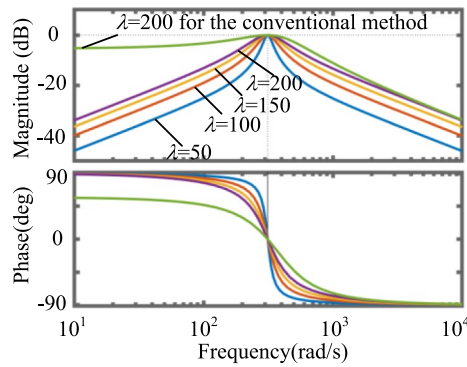


Fig. 4. Bode diagram of  $G_3$ .

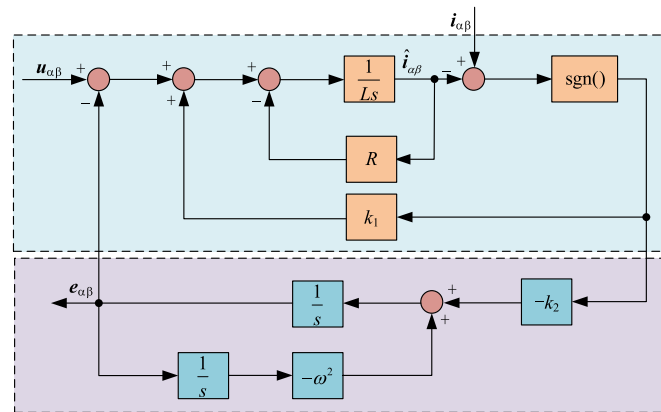


Fig. 5. Control block diagram of the proposed grid voltage observer.

can be eliminated completely. Moreover,  $\lambda$  can be selected larger to improve the bandwidth of the proposed observer since  $G_{3(s=0)} = 0$  remains unchanged. That are the main advantages of the proposed observer. For the high frequency characteristic, it is seen from Fig. 4 that both the conventional and the proposed observer have a similar magnitude at high frequency region. All the above analyses show the advantages of the proposed grid voltage observer.

To make it more clear, Fig. 5 is given to illustrate the control block diagram of the proposed grid voltage observer. After the grid voltage is observed, a phase-locked loop (PLL) can be utilized to get its phase angle, which can be substituted into (3) to generate the reference current for the AC voltage sensorless predictive current control system.

### Proposed current DC offset estimation method

Although the proposed grid voltage observer shown in Sect. “Proposed grid voltage observation method” can eliminate the influences of the current DC offset, it does not consider the effects of the current DC offset on the predictive current control system. In this Section, the effects of the DC offset on the current control is analyzed, and a new observer is designed to estimate and compensate this DC offset error.

### Effects analysis of current DC offset

Due to the impacts of the current sampling circuits, both current gain errors and DC offset errors can be generated<sup>36</sup>. In this paper, only the DC offset errors are considered.

If only  $i_a$  and  $i_b$  are measured with unexpected DC offset errors, it can be deduced that

$$\begin{cases} i_{a\_m} = i_a + i_{a\_offset} \\ i_{b\_m} = i_b + i_{b\_offset} \\ i_{c\_m} = -i_a - i_b - i_{a\_offset} - i_{b\_offset} \end{cases} \quad (27)$$

where  $i_{a\_m}$ ,  $i_{b\_m}$ , and  $i_{c\_m}$  are the measured currents,  $i_{a\_offset}$  and  $i_{b\_offset}$  are the unexpected DC offset errors, and  $i_a$ ,  $i_b$ , and  $i_c$  are the actual currents.

By transforming  $i_{a\_m}$ ,  $i_{b\_m}$ , and  $i_{c\_m}$  to the stationary  $\alpha\beta$  reference frame, it is obtained that

$$\begin{cases} i_{\alpha\_m} = i_{\alpha} + i_{a\_offset} \\ i_{\beta\_m} = i_{\beta} + \frac{\sqrt{3}}{3}(i_{a\_offset} + 2i_{b\_offset}) \end{cases} \tag{28}$$

where

$$\begin{cases} i_{\alpha} = i_a \\ i_{\beta} = \frac{\sqrt{3}}{3}(i_b - i_c) \end{cases} \tag{29}$$

When  $i_{\alpha\_m}$ , and  $i_{\beta\_m}$  are taken as the feedbacks, under the action the predictive current control, it will become that

$$\begin{cases} i_{\alpha\_m} = i_{\alpha}^* \\ i_{\beta\_m} = i_{\beta}^* \end{cases} \tag{30}$$

As a result, due to the unexpected DC offset errors, the actual currents will become to

$$\begin{cases} i_{\alpha} = i_{\alpha}^* - i_{a\_offset} \\ i_{\beta} = i_{\beta}^* - \frac{\sqrt{3}}{3}(i_{a\_offset} + 2i_{b\_offset}) \end{cases} \tag{31}$$

From (31) it is seen that once there are some unexpected DC offset errors, there will be some obvious current control errors too, deteriorating the control performance evidently. Thus, it is very necessary to study the current DC offset error estimation and compensation methods.

### Design of DC offset estimation method

When considering the effects of the current DC offset under AC voltage sensorless condition, (32) can be deduced by substituting (28) into (2).

$$\begin{cases} L \frac{di_{\alpha\_m}}{dt} - L \frac{di_{a\_offset}}{dt} = u_{\alpha} - R(i_{\alpha\_m} - i_{a\_offset}) - \hat{e}_{\alpha} \\ L \frac{di_{\beta\_m}}{dt} - L \frac{d\frac{\sqrt{3}}{3}(i_{a\_offset} + 2i_{b\_offset})}{dt} = \\ u_{\beta} - R(i_{\beta\_m} - \frac{\sqrt{3}}{3}(i_{a\_offset} + 2i_{b\_offset})) - \hat{e}_{\beta} \end{cases} \tag{32}$$

By rewriting (32) with lumped DC offset errors, (33) is obtained.

$$L \frac{d\mathbf{i}_{\alpha\beta\_m}}{dt} = \mathbf{u}_{\alpha\beta} - R\mathbf{i}_{\alpha\beta\_m} - \hat{\mathbf{e}}_{\alpha\beta} + \mathbf{d}_{\alpha\beta} \tag{33}$$

where  $\mathbf{d}_{\alpha\beta} = [d_{\alpha}, d_{\beta}]^T$  and

$$\begin{cases} d_{\alpha} = Ri_{a\_offset} + L \frac{di_{a\_offset}}{dt} \\ d_{\beta} = R \frac{\sqrt{3}}{3}(i_{a\_offset} + 2i_{b\_offset}) + L \frac{d\frac{\sqrt{3}}{3}(i_{a\_offset} + 2i_{b\_offset})}{dt} \end{cases} \tag{34}$$

Since the current DC offset are often DC signals, (34) can be further simplified as

$$\begin{cases} d_{\alpha} = Ri_{a\_offset} \\ d_{\beta} = R \frac{\sqrt{3}}{3}(i_{a\_offset} + 2i_{b\_offset}) \end{cases} \tag{35}$$

From (35) it is seen that if  $d_{\alpha}$  and  $d_{\beta}$  are observed, the unexpected DC offset errors  $i_{a\_offset}$ , and  $i_{b\_offset}$  can be calculated. So, in this Section, a new sliding mode observer is designed to observe the lumped DC offset errors  $\mathbf{d}_{\alpha\beta}$ .

Based on (33), a sliding mode lumped DC offset observer is designed as

$$\begin{cases} L \frac{d\hat{\mathbf{i}}_{\alpha\beta\_m}}{dt} = \mathbf{u}_{\alpha\beta} - R\hat{\mathbf{i}}_{\alpha\beta\_m} - \hat{\mathbf{e}}_{\alpha\beta} + \hat{\mathbf{d}}_{\alpha\beta} \\ \hat{\mathbf{d}}_{\alpha\beta} = k_3 \text{sgn}(\mathbf{i}_{\alpha\beta\_m} - \hat{\mathbf{i}}_{\alpha\beta\_m}) \end{cases} \tag{36}$$

where  $\hat{\mathbf{i}}_{\alpha\beta\_m} = [\hat{i}_{\alpha\_m}, \hat{i}_{\beta\_m}]^T$  is the estimated current,  $\hat{\mathbf{d}}_{\alpha\beta} = [\hat{d}_{\alpha}, \hat{d}_{\beta}]^T$  and  $k_3$  is the observer gains.

According to (33) and (36), it is deduced that

$$L \frac{d(i_{\alpha\beta\_m} - \hat{i}_{\alpha\beta\_m})}{dt} = -R(i_{\alpha\beta\_m} - \hat{i}_{\alpha\beta\_m}) + d_{\alpha\beta} - \hat{d}_{\alpha\beta} \tag{37}$$

To ensure the stability of the proposed lumped DC offset observer, a Lyapunov function is designed as (38) firstly.

$$V_2 = \frac{1}{2}(i_{\alpha\beta\_m} - \hat{i}_{\alpha\beta\_m})^2 \tag{38}$$

To ensure the stability,  $dV_2/dt$  should be less than zero. Using the same analysis method as Sect. “Stability analysis”, it is concluded that

$$k_3 > |d_{\alpha\beta}| \tag{39}$$

That’s the selection method of the gain  $k_3$ .

Finally, to get the lumped DC offset with reduced sliding mode chattering, a low-pass filter is utilized, and the observed  $\hat{d}_{\alpha\beta}$  is further expressed as

$$\hat{d}_{\alpha\beta} = \frac{\omega_c}{s + \omega_c} k_3 \text{sgn}(i_{\alpha\beta\_m} - \hat{i}_{\alpha\beta\_m}) \tag{40}$$

where  $\omega_c$  is the cut-off frequency of the low-pass filter.

For clarity, Fig. 6 is given to illustrate the control block diagram of the proposed lumped DC offset observer.

**The proposed AC voltage sensorless control method with enhanced robustness against DC offset error**

Once both the grid voltage  $\hat{e}_{\alpha\beta}$  and the lumped DC offset  $\hat{d}_{\alpha\beta}$  are observed, the predictive current control method can be redesigned to achieve AC voltage sensorless control with enhanced robustness against current DC offset error. The detailed execution steps of the proposed method are depicted below.

Step 1: Observe the grid voltage  $\hat{e}_{\alpha\beta}$  based on (17) and calculate its phase angle.

Step 2: Estimate the lumped DC offset  $\hat{d}_{\alpha\beta}$  based on (36) and (40).

Step 3: Predict the current  $i_{\alpha\beta}(k+1)$  based on (41) using the optimal voltage vector selected in the last control period.

$$i_{\alpha\beta}(k+1) = (1 - \frac{R}{L}T_s)(i_{\alpha\beta}(k) - \frac{\hat{d}_{\alpha\beta}}{R}) + \frac{T_s}{L}(u_{\alpha\beta}(k) - \hat{e}_{\alpha\beta}(k)) \tag{41}$$

Step 4: Predict the current  $i_{\alpha\beta}(k+2)$  based on (42) using the eight voltage vectors of the grid-tied inverter.

$$i_{\alpha\beta}(k+2) = (1 - \frac{R}{L}T_s)(i_{\alpha\beta}(k+1) - \frac{\hat{d}_{\alpha\beta}}{R}) + \frac{T_s}{L}(u_{\alpha\beta}(k+1) - \hat{e}_{\alpha\beta}(k+1)) \tag{42}$$

Step 5: Calculate the reference current based on (3) using the estimated phase angle of the grid voltage, and calculate the cost function shown in Fig. 2 using the eight predicted currents.

Step 6: Evaluate the cost function shown in Fig. 2 and select the voltage vector with minimized cost function as the optimal one, which is finally used to control the grid-tied inverter.

Based on the above steps, AC voltage sensorless control with enhanced robustness against current DC offset error is ensured.

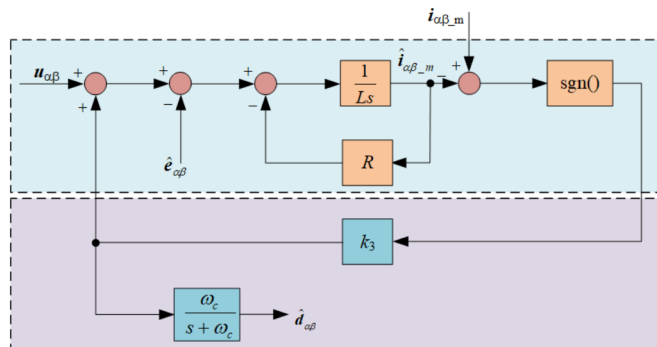


Fig. 6. Control block diagram of the proposed lumped DC offset observer.

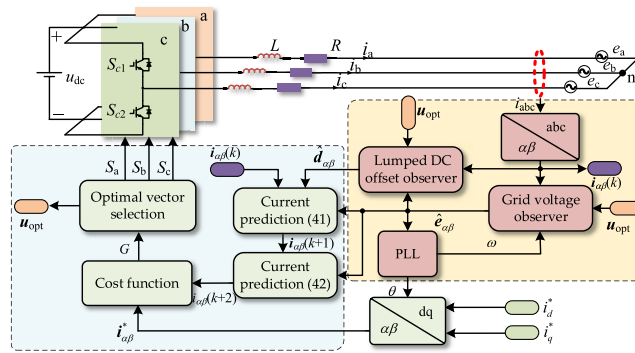


Fig. 7. Whole control block diagram of the proposed predictive control method.

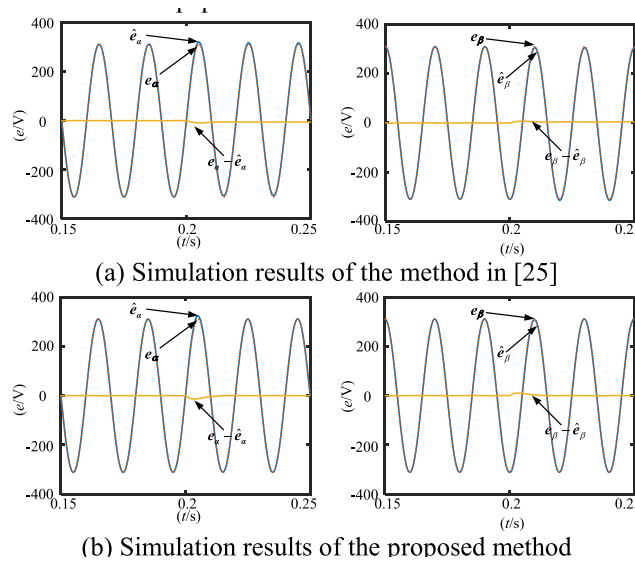


Fig. 8. Simulation results of the two methods with injected voltage DC offset.

For clarity, Fig. 7 is given to illustrate the whole control block diagram of the proposed predictive control method in this paper.

### Simulation and experimental studies

To verify the effectiveness of the proposed AC voltage sensorless control method with enhanced robustness against current DC offset error in this paper, comparative simulation and experimental studies are carried out in this Section based on MATLAB/Simulink and HIL experimental platform. In simulation and experimental studies, the DC voltage is set as 600 V, and the line-to-line AC voltage is set as 380 V. The inductance is set as 20mH, and the resistance is 0.01Ω. The control frequency is set as 10 kHz, and the deadtime is 2 μs. The detailed simulation and experimental results with analysis are shown below.

#### Simulation study of the proposed grid voltage observer with DC offsets

To show the effectiveness and advantages of the proposed grid voltage observer in this paper, a simulation study is carried out. The performance of the proposed method is compared with the method in<sup>25</sup>. In this simulation, a DC offset of 20 V is injected into  $u_{\alpha}$  and a DC offset of -15V is injected into  $u_{\beta}$ . The results are shown in Fig. 8. It is seen that when DC offset is injected, there is a small grid voltage observation error for the method in<sup>25</sup>, while the estimation error of the proposed method is almost 0 at steady-state. That's because the conventional method cannot remove the influences of the DC offset, while the proposed method is immune to DC offset, showing the effectiveness and advantages of the proposed grid voltage observer in this paper.

#### Simulation study of the proposed DC offset estimation method

To show the effectiveness of the proposed current DC offset estimation method, another simulation study is carried out, where a DC offset of 5 A is injected into  $i_{\alpha}$ , while a DC offset of -2.5A is injected into  $i_{\beta}$ . Figure 9 shows the simulation result of the estimated current DC offset using the proposed method. Figure 10 shows

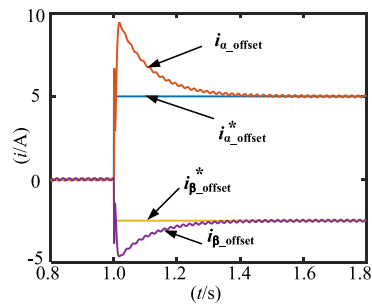


**Fig. 9.** Simulation results of the estimated current DC offsets  $i_{\alpha\_offset}$  and  $i_{\beta\_offset}$ .

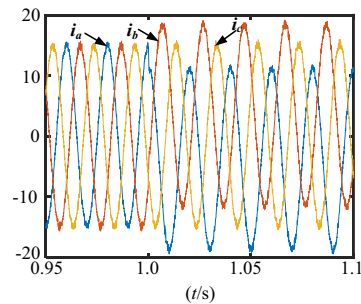


**Fig. 10.** Simulation results of the actual current without compensation.

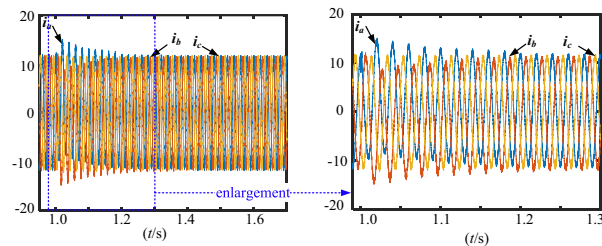


**Fig. 11.** Simulation results of the actual current with compensation.

the actual currents without DC offset compensation, while Fig. 11 illustrates the results when the DC offset is compensated using the proposed method.

It is clear to see from Fig. 9 that the current DC offset is well estimated by the proposed method, indicating the effectiveness of the proposed method.

It is seen from Fig. 10 that obvious DC offsets are generated in the actual current when there is no compensation, while the DC offsets are reduced to zero for the proposed method with compensation, as depicted in Fig. 11, which further indicates the advantages of the proposed method.

### Simulation study of the proposed AC voltage sensorless control method

To further show the robustness against current DC offsets of the proposed AC voltage sensorless control method, another comparative simulation study is implemented. For the conventional method, both the actual grid voltage and grid current are measured and used for predictive current control. Due to the influences of the sampling circuits, both the measured grid voltage and grid current may contain unexpected DC offsets, affecting the predictive current control performance. For the proposed method, only the current is measured, which may contain DC offsets. However, this paper not only proposed a grid voltage observation method, but also designed a current DC offset estimation and compensation method, which can remove the influences of the unexpected DC offsets. To verify this fact, in this simulation, the control performance of the conventional method as well as the proposed one are tested and compared with unexpected DC offsets. The results are shown in Fig. 12 and 13, respectively. In this simulation, to simulate the effects of the sampling circuits, a DC offset of 20 V is injected into the measured grid voltage  $u_a$ . Meanwhile, a DC offset of 5 A is injected into the measured grid current  $i_a$ , and a DC offset of  $-2.5$  A is injected into the measured grid current  $i_\beta$ .

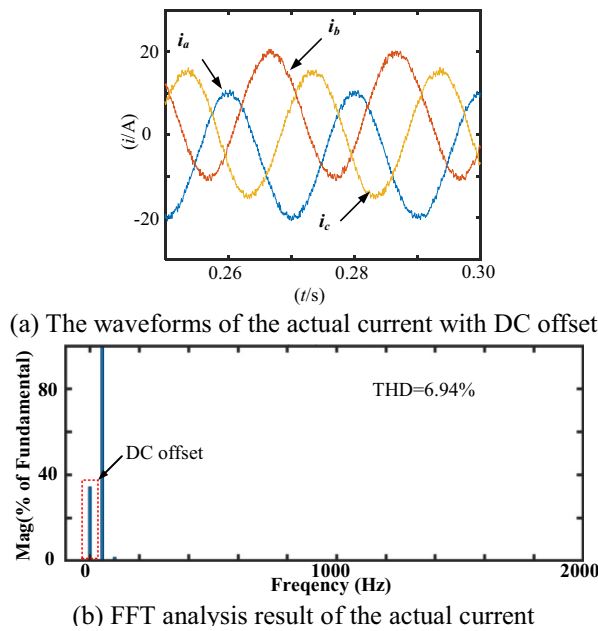


Fig. 12. Simulation results of the conventional method with DC offset.

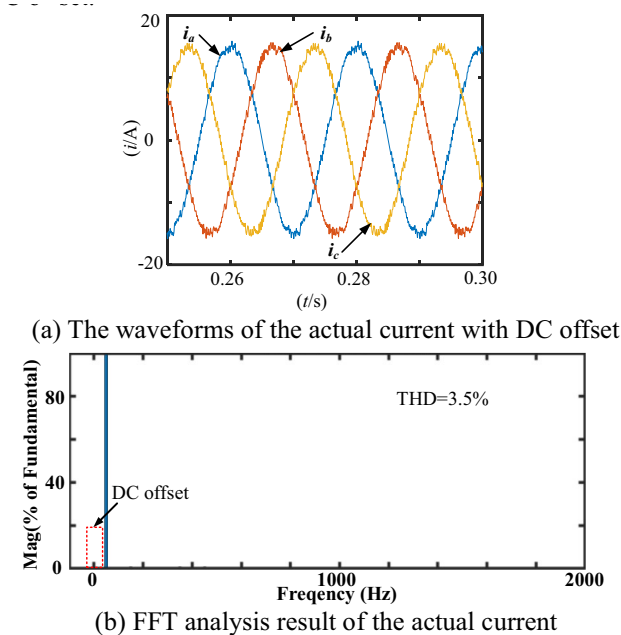


Fig. 13. Simulation results of the proposed method with DC offset.

It is seen from Fig. 12 that the conventional method is very sensitive to current DC-offset. Without compensation, the THD of the current is quite large with DC offset. For the proposed method in this paper, it is seen from Fig. 13 that the THD of the current is quite small without DC offset, indicating the effectiveness of the proposed method in this paper again.

### Experimental study of the proposed grid voltage observer with DC offsets

To further show the effectiveness of the proposed method in this paper, experimental studies are carried out based on HIL experimental platform shown in Fig. 14, which is based on the Xilinx Kintex-7 160 T field programmable gate array controller.

First, an experimental study is carried out to show the robustness of the proposed grid voltage observer against the DC offsets. In this experiment, a DC offset of 20 V is injected into  $u_a$  at  $t_1$  instant and a DC offset of -15V is injected into  $u_b$  at  $t_2$  instant. The experimental results are shown in Fig. 15 and 16.

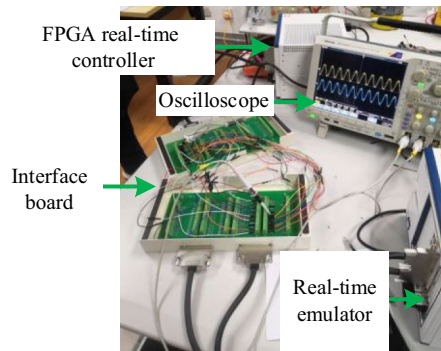


**Fig. 14.** Experimental platform.

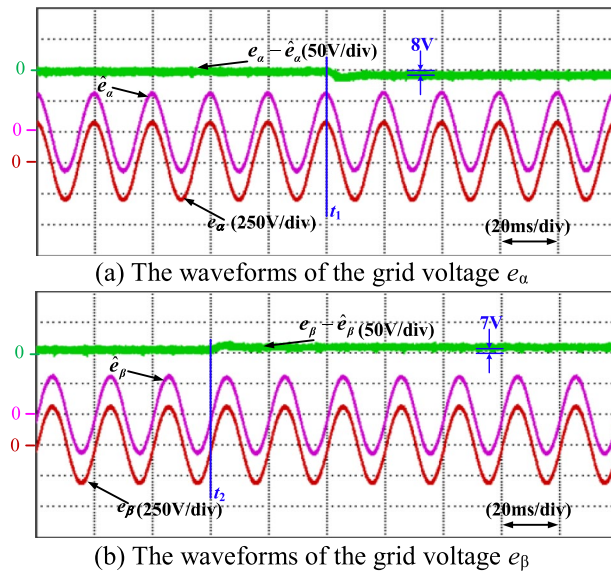


**Fig. 15.** Experimental results of the method in<sup>25</sup> with injected voltage DC offset.

It is seen from Fig. 15 that when DC offsets are injected suddenly, obvious grid voltage observation errors are generated, which are about 8 V and 7 V respectively. The results show that the conventional method in<sup>25</sup> is very sensitive to DC offset, resulting in poor grid voltage observation performance.

It is seen from Fig. 16 that when DC offsets are injected unexpectedly, obvious grid voltage observation errors are also generated suddenly. Fortunately, it is seen that the error  $e_\alpha - \hat{e}_\alpha$  at  $t_1$  instant is decreased to zero fast, and the error  $e_\beta - \hat{e}_\beta$  at  $t_2$  instant is also decreased to zero quickly. At steady state, the grid voltage observation errors are both 0 for the proposed method, which shows that the proposed grid voltage observer is robust against DC offsets, indicating its better grid voltage observation precision.

### Experimental study of the proposed DC offset estimation method

Second, to show the effectiveness of the proposed current DC offset estimation method, another experimental study is carried out, where a DC offset is suddenly injected into the current at  $t_3$  instant, where the measured grid voltage is used for predictive control. The estimated current DC offsets are shown in Fig. 17. Figure 18 shows the current waveforms without DC offset compensation, while Fig. 19 shows the current waveforms with the proposed DC offset estimation and compensation method.

It is seen from Fig. 17 that by using the proposed sliding mode lumped DC offset observer, the unexpected current DC offsets can be estimated precisely and quickly. The convergence time is about 340ms and the steady-state estimation error is very small. That shows the validity of the proposed current DC offset estimation method.

From Fig. 18 it is seen that under the effects of the injected current DC offsets, the actual current will have obvious DC offsets if there is no compensation, deteriorating the control performance heavily. That shows the badly effects of the DC offsets as well as the necessary and significance to estimate and compensate the unexpected current DC offsets.

From Fig. 19 it is seen that when unexpected current DC offsets are injected at  $t_3$  instant, large current control errors are generated suddenly. Fortunately, under the action of the proposed DC offset estimation and

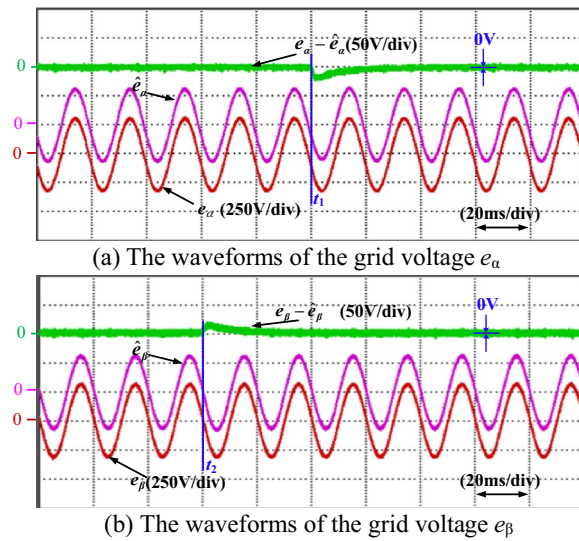


Fig. 16. Experimental results of the proposed method in this paper with injected voltage DC offset.

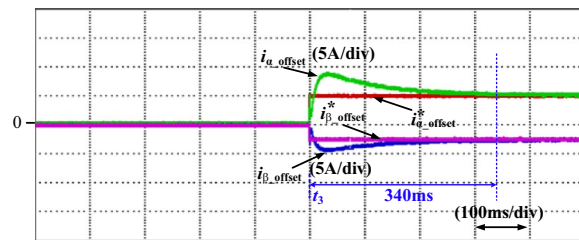


Fig. 17. Experimental results of the estimated current DC offsets  $i_{\alpha\_offset}$  and  $i_{\beta\_offset}$ .

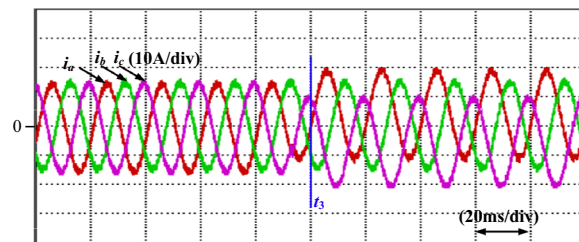


Fig. 18. Experimental results of the actual current without compensation.

compensation algorithm, the current control errors are reduced quickly, and the three-phase current goes back to steady state without DC offset. That shows the effectiveness of the proposed DC offset estimation and compensation algorithm.

**Experimental study of the proposed AC voltage sensorless control method**

Third, to further show the robustness against current DC offsets of the proposed AC voltage sensorless control method, another comparative experimental study is also implemented. The experiment condition is the same with the simulation condition depicted in Sect. “Simulation study of the proposed AC voltage sensorless control method”. The results are shown in Fig. 20 and 21, respectively.

From Fig. 20 it is seen that the actual currents of the conventional method are distorted with obvious DC offset. That’s because the voltage DC offset affects the phase angle of the grid voltage, resulting in distorted reference currents. Meanwhile, the current DC offset affects the actual currents. As a result, both distortion and DC offset are generated. Consequently, the THD of the current is increased to 7.8%.

From Fig. 21 it is seen that although voltage and current DC offsets are injected, the actual currents at steady state are still satisfactory without DC offset and distortion. The THD of the actual current is 4.6%. Compared

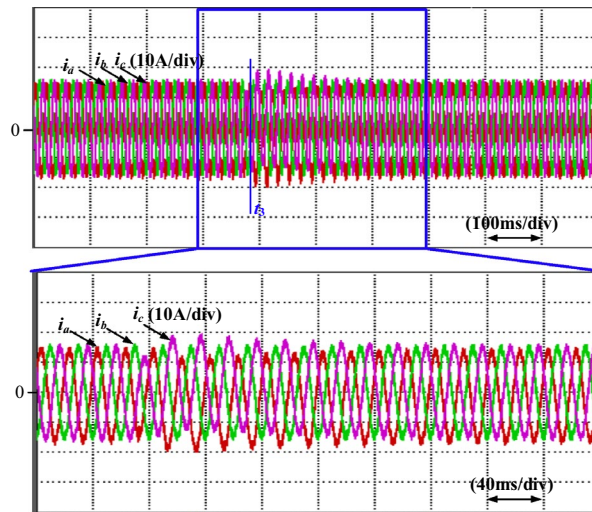
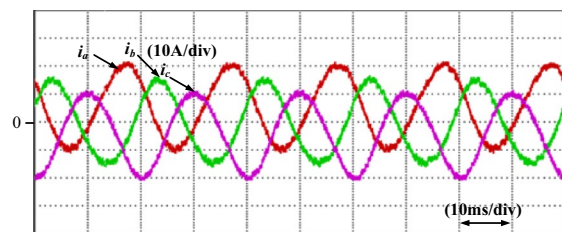
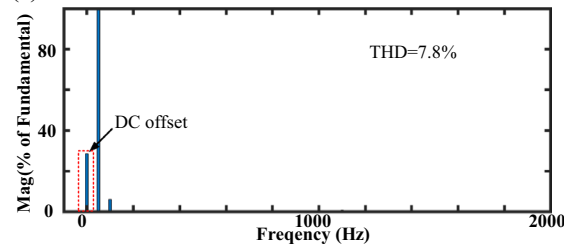


Fig. 19. Experimental results of the actual current with compensation.



(a) The waveforms of the actual current with DC offset



(b) FFT analysis result of the actual current

Fig. 20. Experimental results of the conventional method with DC offset.

Fig. 20 with Fig. 21, it is clear to see that the proposed method in this paper has strong robustness against DC offsets, improving the current control performance significantly.

All the above experimental results verify the effectiveness and superiority of the proposed AC voltage sensorless control method with enhanced robustness against DC offsets.

### Experimental study of the parameter sensitivity

As a model-based method, the proposed AC voltage sensorless predictive current control method relies on the parameters of the grid-tied inverter. Typically, the inductance often has a large influence on the proposed observers<sup>37</sup>. So, in this section, the influences of the inductance on the proposed grid voltage observer and the current DC offset observer are tested under different conditions.

First, the influences of the inductance on the proposed grid voltage observer are tested, where the inductance used in the control algorithm is changed from 0.02H to 0.015H, 0.02H, and 0.025H.

Figure 22(a) illustrates the results of the conventional method, while Fig. 22(b) depicts the results of the proposed method.

It is seen that when there is an inductance error, obvious grid voltage observation errors are generated for the two methods. That shows the sensitivity of the two grid voltage observers, which are the common demerits of the model-based observers. Fortunately, the grid voltage observation error is quite small, which does not have significant effects on the AC voltage sensorless control.

To overcome the influences of the inductance, inductance estimation methods should be further studied in the future.

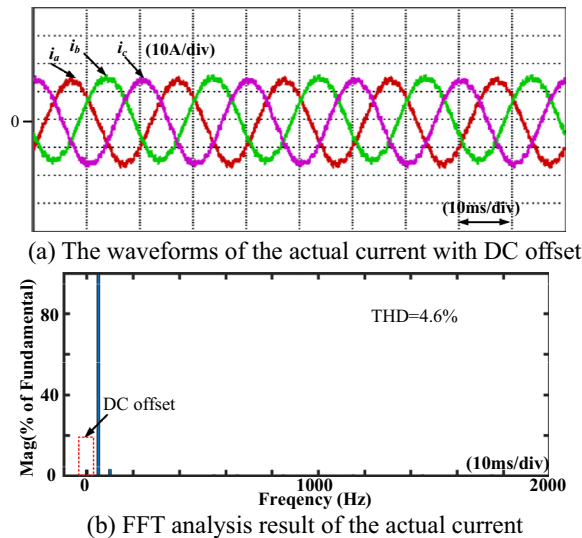


Fig. 21. Experimental results of the proposed method with DC offset.

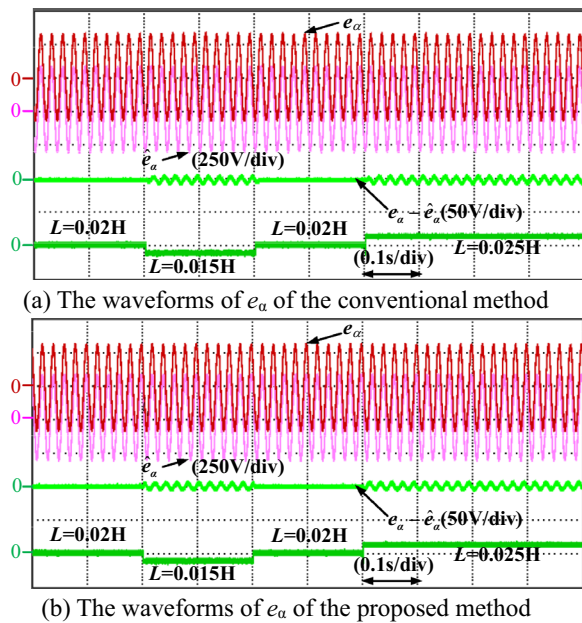


Fig. 22. Experimental results of the observed grid voltage when the inductance changes.

Second, the influences of the inductance on the proposed current DC offset observer are tested, where the inductance used in the control algorithm is changed from 0.02H to 0.015H, 0.02H, 0.015H and 0.025H. The results are shown in Fig. 23.

It is seen that when a current DC offset of 5 A is injected suddenly, the observed current DC offset can converge to 5 A quickly. Then, when the inductance changes suddenly, the observed current DC offset can still converge to 5 A quickly at steady state. That means the proposed current DC offset estimation method is insensitivity to the inductance mismatches at steady state, showing its advantages and superiorities.

### Comparative analysis

To compare the advantages of the proposed method with other methods presented in the past, a comparative analysis is conducted in this section, as shown in Table 1.

For the methods proposed in<sup>20,21</sup>, although AC voltage sensorless predictive current control is achieved, both the observed AC voltage and the predictive current control system are sensitive to current DC offset.

For the methods proposed in<sup>25</sup>, AC voltage sensorless predictive current control is also achieved. However, the designed AC voltage observer has a weak band-pass characteristic. That means this observer only can reduce

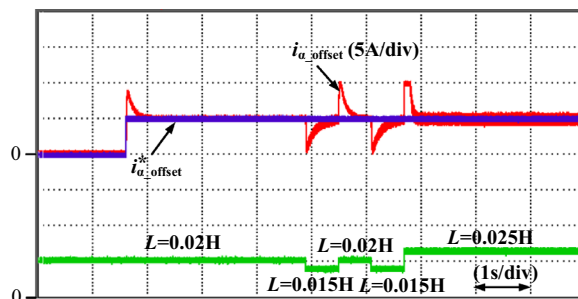


**Fig. 23.** Experimental results of the observed current DC offset when the inductance changes.

Methods	AC voltage sensorless	Insensitive to current DC offset
<sup>20,21</sup>	Yes	No
<sup>25</sup>	Yes	No (Only can reduce the effects of current DC offset to a certain extent)
<sup>28–32</sup>	No	Yes
The proposed method	Yes	Yes

**Table 1.** Comparative analysis.

the effects of current DC offset to a certain extent, rather than eliminating. Moreover, the influences of the DC errors on the predictive current control are not addressed in this paper.

For the methods proposed in<sup>28–32</sup>, the current DC offset is estimated and compensated using different methods. However, in these methods, AC voltage sensorless control cannot be achieved.

Up to now, few papers have studied the AC voltage sensorless predictive current control method for grid-tied inverter with enhanced robustness against current DC offset. So, in this paper, new methods are proposed.

First, an improved grid voltage observer is proposed, which can eliminate the effects of the current DC offset. So, compared with the methods in<sup>20,21</sup>, and<sup>25</sup>, AC voltage sensorless control is achieved immune to current DC offset.

Second, a new DC offset observer is designed in this paper, which can observe the current DC-offset well without using AC voltage sensors. So, AC voltage sensorless predictive current control immune to current DC offset is also achieved.

In a word, for the proposed method in this paper, both the influences of the current DC offset on the grid voltage observation and the predictive current control are eliminated at the same time, overcoming the drawbacks of the methods in<sup>20,21,25</sup>, and<sup>28–32</sup>.

## Conclusion

In this paper, a new AC voltage sensorless predictive current control method for grid-tied inverter with enhanced robustness against DC offset is proposed. First, a new grid voltage observer is developed based on the backstepping design approach, which can remove the effects of the current DC offsets on the grid voltage observation. Second, a new lumped DC offset observer is designed, which can eliminate the influences of the unexpected current DC offset on the predictive current control. Third, comparative experimental studies are carried out, which verify the effectiveness of the proposed methods in this paper.

Meanwhile, it should be noted that the mismatch of the inductance has an obvious influence on the proposed grid voltage observer, which is a common drawback of the model-based observers. So, in the future, it is necessary to further study the inductance estimation method to enhance the parameter robustness of the proposed method in this paper.

## Data availability

All datasets used and/or analysed during the current study available from the corresponding author on reasonable request.

Received: 14 September 2025; Accepted: 17 October 2025

Published online: 21 November 2025

## References

1. L. Guo, H. Ma, Z. Wu et al. A fast-anti-disturbance enhanced finite-time disturbance observer-based speed control method for surface-mounted permanent magnet synchronous motor. *Electr Eng.* published online. (2025).
2. Guo, L., Xu, W., Jin, N. & Xiao, H. A DC-offset removed sensorless control method for PMSM based on SMO with an improved prefilter and a speed immune position error compensation strategy. *IEEE Trans. Power Electron* **40**, 5163–5176 (2025).
3. Sai Sampath KumarSureshLenine, P. P. D. Performance improvement of predictive voltage control for interlinking converters of integrated microgrid. *Meas.: Sens.* **33**, 101196 (2024).

4. Jiang, S., Du, L., Li, Y., Yang, L. & Luo, B. LCL APF control strategy based on model predictive control. *Front. Energy Res.* **12**, 1423199 (2024).
5. Zhang, Z. et al. An improved robust model predictive and repetitive combined control for three-phase four-leg active power filters with fixed switching frequency. *Energy Rep.* **8**, 14347–14361 (2022).
6. Sreedhar, R., Karunanithi, K. & Ramesh, S. Design, implementation and empirical analysis of a cascaded hybrid MPPT controller for grid tied solar photovoltaic systems under partial shaded conditions. *Meas.: Sens.* **31**, 100961 (2024).
7. Guo, L., Li, Y., Jin, N., Dou, Z. & Wu, J. Sliding mode observer-based AC voltage sensorless model predictive control for grid-connected inverters. *IET Power Electron.* **13**, 2077–2085 (2020).
8. Sang, W. et al. A novel robust active damping control strategy based on  $H_\infty$  loop shaping for the grid-tied LCL inverter. *Front. Energy Res.* **12**, 1473060 (2024).
9. Tan, W. & Fu, C. Linear active disturbance-rejection control: analysis and tuning via IMC. *IEEE Trans. Ind. Electron.* **63**, 2350–2359 (2016).
10. Scoltock, J., Geyer, T. & Madawala, U. K. A model predictive direct current control strategy with predictive references for mv grid-connected converters with LCL-filters. *IEEE Trans. Power Electron.* **30**, 5926–5937 (2015).
11. Jin, N., Chen, M., Guo, L., Li, Y. & Chen, Y. Double-vector model-free predictive control method for voltage source inverter with visualization analysis. *IEEE Trans. Ind. Electron.* **69**, 10066–10078 (2022).
12. Santos, T. B. D. et al. Robust finite control set model predictive current control for induction motor using deadbeat approach in stationary frame. *IEEE Access* **11**, 13067–13078 (2023).
13. Long, Z., Zhu, W., Yang, K. T., Chong, J. R. & Guerrero, J. M. Gradient descent optimization based parameter identification for FCS-MPC control of LCL-type grid connected converter. *IEEE Trans. Ind. Electron.* **69**, 2631–2643 (2022).
14. Li, Y., Li, W., Guo, L., Jin, N. & Lu, F. Current sensor-less virtual synchronous generator model predictive control based on sliding mode observer. *IEEE Access* **9**, 17898–17908 (2021).
15. Wei, Y. et al. Model-free predictive control using sinusoidal generalized universal model for PMSM drives. *IEEE Trans. Ind. Electron.* **71**, 13720–13731 (2024).
16. Gao, X. et al. Model predictive control of a modular multilevel converter considering control input constraints. *IEEE Trans. Power Electron.* **39**, 636–648 (2024).
17. Xu, W. et al. A review of finite control set model predictive control for linear machines. *IET Electr. Power Appl.* **18**, 1567–1583 (2024).
18. Baig, M. A., Kashif, S. A. R., Gulzar, M. M., Alqahtani, M. & Khalid, M. Improved hybrid sphere decoding algorithm for long horizon finite control set model predictive control of grid-tied inverter. *Energy Rep.* **10**, 3229–3239 (2023).
19. de Assumpcao Ribeiro, B., Werneck, M. M. & da Silva-Neto, J. L. Novel optimization algorithm to demodulate a PZT-FBG sensor in ac high voltage measurements. *IEEE Sens. J.* **13**, 1259–1264 (2013).
20. Guo, L., Jin, N., Li, Y. & Luo, K. A model predictive control method for grid-connected power converters without AC voltage sensors. *IEEE Trans. Ind. Electron.* **68**, 1299–1310 (2021).
21. Guo, L. et al. An inductance online identification method for model predictive control of V2G inverter with enhanced robustness to grid frequency deviation. *IEEE Trans. Transp. Electrification.* **8**, 1575–1589 (2022).
22. Sun, Y., Li, Z., Zhang, Y., Li, Y. & Zhang, Z. A time-domain virtual-flux based predictive control of modular multilevel converters for offshore wind energy integration. *IEEE Tran. on Energy Conv.* **37**, 1803–1814 (2022).
23. Li, C., Hu, J. & Zhao, M. Grid-voltage sensorless predictive current control of three-phase PWM rectifier with fast dynamic response and high accuracy. *CPSS Trans. Power Electron. Appl.* **8**, 269–277 (2023).
24. Le, V.-T. & Lee, H.-H. Grid-voltage sensorless model-free predictive current control for PWM Rectifiers with measurement noise suppression. *IEEE Trans. Power Electron.* **37**, 10681–10697 (2022).
25. Yang, H., Zhang, Y., Zhang, N., Walker, P. D. & Gao, J. A voltage sensorless finite control set-model predictive control for three-phase voltage source PWM rectifiers. *Chin. J. Electr. Eng.* **2**, 52–59 (2016).
26. Zheng, C., Dragičević, T. & Blaabjerg, F. Current-sensorless finite-set model predictive control for LC-filtered voltage source inverters. *IEEE Trans. Power Electron.* **35**, 1086–1095 (2020).
27. L. Guo, Y. Jing, Y. Wang, et al. Model-free predictive current control for a new neutral point connected open-end winding induction motor based on an improved sliding mode observer. *Electr Eng.* published online. (2025).
28. Lee, K.-W. & Kim, S.-I. Dynamic performance improvement of a current offset error compensator in current vector-controlled SPMSM drives. *IEEE Trans. Ind. Electron.* **66**, 6727–6736 (2019).
29. Kim, S.-I., Kim, J.-Y. & Lee, K.-W. Current measurement offset error compensation scheme considering saturation of current controller in SPMSM drives. *IEEE Access* **11**, 17233–17240 (2023).
30. Lee, S., Kim, H. & Lee, K. Current measurement offset error compensation in vector-controlled SPMSM drive systems. *IEEE J. Emerg. Select. Topics Power Electron.* **10**, 2619–2628 (2022).
31. Zuo, Y. et al. A novel current measurement offset error compensation method based on the adaptive extended state observer for IPMSM drives. *IEEE Trans. Ind. Electron.* **71**, 3371–3382 (2024).
32. Hwang, S.-H. DC offset error compensation of current sensor for single-phase permanent magnet synchronous motor drives. *J. Electr. Eng. Technol.* **19**, 547–555 (2024).
33. Wu, Z. et al. A robust inductance estimation method for model predictive control of grid-connected inverters. *IEEE Trans. Ind. Electron.* **72**, 589–599 (2025).
34. Cao, L. et al. A dual-vector modulated model predictive control method for voltage source inverters with a new duty cycle calculation method. *Energies* **13**, 4200 (2020).
35. Zhang, Y., Pen, H. & Zhang, X. Stability control of grid-connected converter considering phase-locked loop frequency coupling effect. *Energies* **17**, 3438 (2024).
36. Retianza, D. V., van Duivenbode, J. & Huisman, H. Plant-independent current sensor gain error compensation for highly dynamic drives. *IEEE Trans. Ind. Electron.* **70**, 9948–9958 (2023).
37. Y. Li, Z. Liu, L. Guo, et al. An enhanced adaptive inductance estimator for predictive current control strategy of grid-tied inverters. *Electr Eng.* published online. (2025).

## Author contributions

Conceptualization, Guolin Zhang; methodology, Weidong Dong; validation, Lingfeng Meng; investigation, Jinyuan Li; data curation, Jiqiang Wang; writing—original draft preparation, Guolin Zhang; writing—review and editing, Weidong Dong.

## Declarations

## Competing interests

The authors declare no competing interests.

### Additional information

**Correspondence** and requests for materials should be addressed to W.D.

**Reprints and permissions information** is available at [www.nature.com/reprints](http://www.nature.com/reprints).

**Publisher's note** Springer Nature remains neutral with regard to jurisdictional claims in published maps and institutional affiliations.

**Open Access** This article is licensed under a Creative Commons Attribution-NonCommercial-NoDerivatives 4.0 International License, which permits any non-commercial use, sharing, distribution and reproduction in any medium or format, as long as you give appropriate credit to the original author(s) and the source, provide a link to the Creative Commons licence, and indicate if you modified the licensed material. You do not have permission under this licence to share adapted material derived from this article or parts of it. The images or other third party material in this article are included in the article's Creative Commons licence, unless indicated otherwise in a credit line to the material. If material is not included in the article's Creative Commons licence and your intended use is not permitted by statutory regulation or exceeds the permitted use, you will need to obtain permission directly from the copyright holder. To view a copy of this licence, visit <http://creativecommons.org/licenses/by-nc-nd/4.0/>.

© The Author(s) 2025